arXiv:1411.5702v1 [cond-mat.mes-hall] 20 Nov 2014

The stability and properties of high-buckled two-dimensional tin and lead

Pablo Rivero,[1] Jia-An Yan,[2] Víctor M. García-Suárez,[3] Jaime Ferrer,[3] and Salvador Barraza-Lopez[1]*
1. Department of Physics. University of Arkansas. Fayetteville AR, 72701. USA.
2. Department of Physics, Astronomy and Geosciences. Towson University. Towson, MD 21252 USA.
3. Departamento de Física and Centro de Investigación en Nanociencia y Nanotecnología. Universidad de Oviedo.
(Dated: November 24, 2014)

In realizing practical non-trivial topological electronic phases stable structures need to be determined first. Tin and lead do stabilize an optimal two-dimensional high-buckled phase –a hexagonal-close packed bilayer structure with nine-fold atomic coordination– and they do not stabilize topological fullerenes, as demonstrated by energetics, phonon dispersion curves, and the structural optimization of finite-size samples. The high-buckled phases are metallic due to their high atomic coordination. The optimal structure of fluorinated tin lacks three-fold symmetry and it stabilizes small samples too. It develops two oblate conical valleys on the first Brillouin zone coupling valley, sublattice, and spin degrees of freedom with a novel $\tau_z\sigma_x s_x$ term, thus making it a new 2D platform for valleytronics.

PACS numbers: 73.22-f, 71.70.Ej, 68.55.at

Introduction.- Carbon forms two-dimensional (2D) layers with a hexagonal lattice [1, 2] and silicon, germanium [3], AlAs, AlSb, GaP, InP, GaAs, InAs, GaSb, InSb [4], phosphorus [5], and tin [6–8] are all predicted to form stable low-buckled (LB) hexagonal 2D layers. High-buckled (HB) 2D phases cannot occur for carbon, silicon, nor germanium [3, 9]. Can tin and lead stabilize the HB phase?

Proceeding by direct analogy to silicene and germanene [3], known studies of the electronic properties of 2D tin [6–8, 10] are performed under the implicit assumption that the HB phase is not viable. In addition, the guess structures and the electronic gaps in Ref. [8] had been previously reported [7]. Contrary to common assumption, the HB 2D structures of heavy column-IV elements tin and lead are stable and lower in energy than their LB counterparts, thus representing the true optimal structures of these two-dimensional systems. The structural stability of HB tin and HB lead will have fundamental consequences for the practical realization of substrate-free non-trivial topological phases based from these elements.

The optimal phase of 2D fluorinated stanene is not analogous to tetrahedrally-coordinated graphane [11] as it was postulated in Refs. [7, 8]. Studies of 2D fluorinated tin dismiss the existence of bulk crystalline fluorinated phases stable at room temperature. *There is no indication for tetrahedral coordination of tin atoms* in bulk fluorinated tin [12] and tetrahedral coordination [7, 8] does not yield the most stable 2D fluorinated tin either.

We uncover *six metastable fluorinated phases for 2D tin*, the graphane-like phase [6–8] being one of them. Consistent with the literature in bulk flourinated tin [12, 13], we demonstrate that *two tilted F atoms mediate the interaction among two Sn atoms* in the optimal 2D structure. This stable optimal phase displays two gapped oblate Dirac cones on the first Brillouin zone where valley $\boldsymbol{\tau}$, pseudospin $\boldsymbol{\sigma}$, and spin $\mathbf{s}$ couple as $\tau_z\sigma_x s_x$ [14].

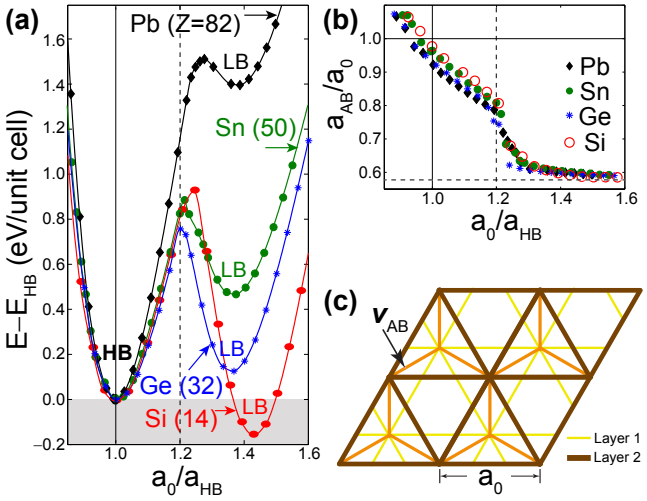

FIG. 1: (Color online.) (a) The high-buckled phase becomes more stable with increasing atomic number. (b) Nearest-neighbor distances $a_{AB} \equiv |\mathbf{v}_{AB}|$ approach the lattice constant a_0 ($a_{AB} \simeq a_0$) at the high-buckled energy minimum; the structure transitions to a low-buckled phase at roughly $1.2a_{HB}$. (c) The high-buckled structure is a HCP bilayer.

Unlike known 2D materials with a hexagonal lattice in which three valleys with momentum directions separated by 120^o rotations are related due to threefold symmetry [15–19], the optimal 2D flourinated tin leads to *strictly two* valleys due to its reduced structural symmetry. This allows an unprecedented specificity in coupling three quantum degrees of freedom around the Fermi energy: the valley, the crystal momentum *including direction*, and the electronic spin.

The results here provided invite to look closely into 2D materials postulated for their remarkable electronic properties that may not realize ground-state, optimal struc-

*Electronic address: sbarraza@uark.edu

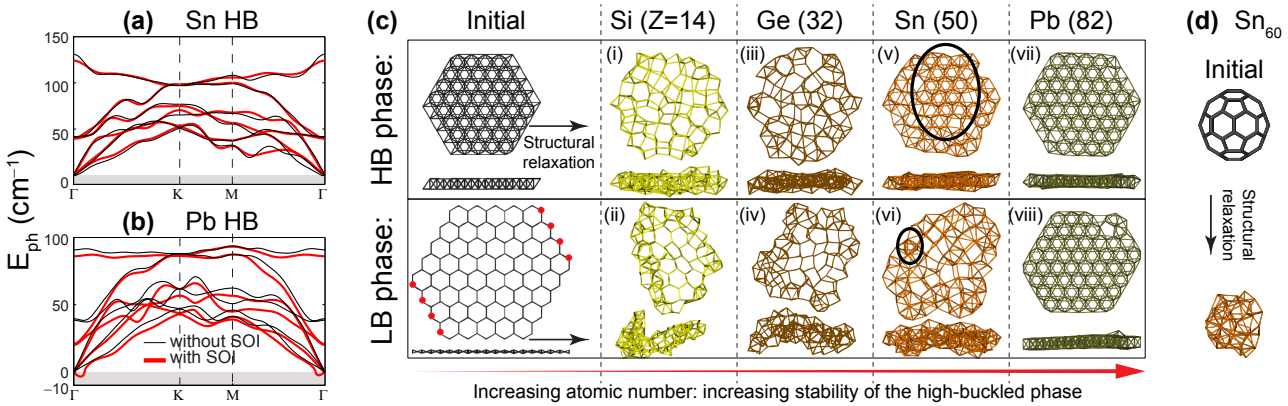

FIG. 2: (Color online.) (a-b) Phonon dispersions $E_{ph}(\mathbf{k})$ for HB tin and lead demonstrate their structural stability; SOI does not change phonon dispersions dramatically. (c) The structural optimization of finite samples reflects previous findings for Si and Ge [3] and helps in confirming the stability of HB tin and HB lead unequivocally: The stanene sample (LB tin) becomes thick and amorphous and the initial LB lead sample turns into HB lead. (d) 2D tin and lead do not realize topological fullerenes.

tures [7, 8].

The HB phase is more favorable than the LB phase with increasing atomic number.- The energetics of column-IV 2D materials on Fig. 1(a) were obtained with the PBE exchange-correlation potential [20] on a version of the *SIESTA* code [21, 22] that includes a self-consistent spin-orbit interaction (SOI) [23]. Our basis sets are of double-zeta plus-polarization size [24]. The trends in Fig. 1 remain regardless of the inclusion of SOI, and were cross-checked with *VASP* calculations [25, 26].

The lattice constant at the HB energy minima a_{HB} is equal to 3.418 Å for tin, and a_{HB}=3.604 Å for lead. These values become 3.413 and 3.575 Å, respectively, when the SOI is included in calculations. These strikingly stable HB structures have not been reported before; lattice parameters in the literature [6–8, 10] are ∼140% larger. Normalization of a_0 in terms of a_{HB} in Figs. 1(a) facilitates an unified display of energetics regardless of atomic species. The vertical dashed line in Figs. 1(a) and 1(b) at about $a_0 \simeq 1.2a_{HB}$ highlights the lattice constant a_0 for which energy barriers separating the LB and the HB phases become largest.

Germanium (with atomic number $Z = 32$) cannot form a HB phase, even though the energy minima of the optimized HB phase is lower than the local minima at the optimal LB phase already [Fig. 1(a)] [3]. This HB minima becomes sizeable deeper and the energy barriers separating these phases become shallower with increasing atomic number. Figure 1(a) invites to ponder whether HB tin and HB lead are stable. In answering this question we address the atomistic coordination of HB phases first.

The optimal HB structure is a hexagonal close-packed bilayer.- HB phases were represented as three-fold coordinated [3], but the relative height Δz among atoms in complementary sublattices A and B increases as the lattice constant a_0 is compressed, so the distance $a_{AB} = \sqrt{a_0^2/3 + \Delta z^2}$ among atoms belonging in complementary sublattices increases towards a_0. Indeed, $a_{AB} = a_0/\sqrt{3}$ for a planar hexagonal unit cell –dashed horizontal line on Fig. 1(b)– but an ideal hexagonal close-packed (HCP) structure has $\Delta z = \sqrt{2}a_0/\sqrt{3}$ yielding $a_{AB} = a_0$ –solid horizontal line on Fig. 1(b) [27]. Numerical results yield $a_{AB} \simeq 0.95a_{HB}$ (solid vertical line on Fig. 1(b)). Thus, six atoms are a distance a_{HB} apart on a triangular lattice, and three atoms belonging on complementary sublattices are separated by $a_{AB} \simeq 0.95a_{HB}$, leading to the nine-fold coordinated HCP bilayer structure [28, 29] on Fig. 1(c). A transition among low- and high-buckled structures occurs around $a_0 \simeq 1.2a_{HB}$ on Fig. 1(b).

HB tin and HB lead are stable.- We show in Figs. 2(a-b) phonon dispersion curves for HB tin and lead [30]. The effect of SOI is small, thus justifying the trends without SOI shown on Fig. 1(a-b) [31]. Similar dispersions were obtained using the *Quantum Espresso* code [32]. The lack of significant negative energies indicates that HB tin and HB lead are indeed stable: The Chemistry of Si and Ge does not translate to Sn and Pb because with increasing atomic number the $s-$orbital lowers its energy with respect to $p-$orbital, thus reducing the $s-p$ hybridization.

The ultimate test of relative stability is a structural optimization of small 2D flakes with initial HB or LB conformations [Fig. 2(c)] where the lines joining atoms reveal their atomistic coordination. The finite-size HB structures have 122 atoms; the LB structures have eight additional atoms (red dots on the LB initial structure) so that all edge atoms are two-fold coordinated. We set a stringent force tolerance cutoff of at least 0.01 eV/Å.

The LB Si and LB Ge samples (subplots *ii* and *iv*) show crumpling originating out from the boundaries yet the hexagonal lattice remains visible around the center of mass after the force relaxation [3]. On the other hand, the amorphous shape and the random-looking atomistic coordination of HB Si and HB Ge (subplots *i* and *iii*) indicate that these phases are unstable [3].

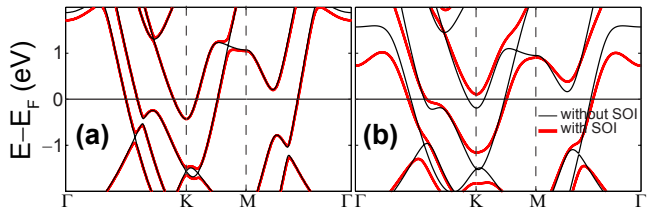

FIG. 3: (Color online.) Electronic dispersion for (a) HB tin and (b) HB lead. The nine-fold atomic coordination of the HB phases is behind the metallic electronic dispersion.

Confirming the structural stability inferred from phonon dispersion curves, HB Sn and HB Pb do stabilize on finite-size samples: Starting from an ideal HB phase, the optimized Sn structure retains the HB coordination within the area highlighted by an oval (Fig. 2(c), subplot *v*). The finite LB Sn sample, on the other hand, crumples upon optimization (Fig. 2(c), subplot *vi*). In fact, the region highlighted by the tiny oval on subplot *vi* in Fig. 2(c) displays the local coordination expected of a HB phase already. Similar conclusions would be reached in Ref. [10] when periodic constraints are removed.

Haldane's honeycomb model has been studied in closed geometries [33] and one of the many candidates for its practical realization is LB tin (stanene). Unfortunately, a fullerene-like Sn_{60} is not stable [Fig. 2(d)] so tin and lead are no-go elements for topological fullerenes. Based on Fig. 1(a) HB lead is extremely stable: It stabilizes finite HB samples with no change in atomic coordination [Fig. 2(c), subplot *vii*] and turns a LB structure onto a HB-coordinated one [Fig. 2(c), subplot *viii*].

Viable electronic materials require stable structures. Tin and lead films have been created experimentally [38–40] and structural aspects must be addressed diligently to realize two-dimensional materials with a strong SOI.

Electronic properties of HB tin and lead.- Graphene, silicene and germanene are three-fold coordinated and have a conical dispersion around the $K-$points with small gaps due to SOI [14, 34–37]. The nine-fold-coordinated 2D HB structures display no conduction gaps [Fig. 3].

Bulk limits.- HCP bilayers could be cleaved out of HCP or FCC bulk structures. Lead forms a FCC structure with interatomic distances of 3.614 Å, which compare favorably with $a_{HB} = 3.575$ and make HB lead stable.

Tin stabilizes a tetragonal structure ($\beta-$tin [41, 42]) and a diamond structure ($\alpha-$tin [43]). The $\beta-$phase is higher in energy than the $\alpha-$phase by $E_\beta - E_\alpha = 0.58$ eV/atom. Every atom on $\beta-$tin has four neighbors at 3.11 Å, two neighbors at 3.26 Å, and four neighbors 3.87 Å apart: these ten atoms are 3.44 Å apart on average. On the nine-fold coordinated HB tin $a_{HB} = 3.42$ Å and $a_{AB} = 3.281$, having an atomistic coordination comparable to bulk $\beta-$tin. The $\alpha-$tin phase has four neighbors 2.89 Å apart, which compares well to $a_{Sn-Sn} = 2.85$ Å for a 2D LB structure. Importantly, in two-dimensions energetics switch and the HB phase –compatible with bulk $\beta-$tin– is more stable than LB tin –compatible with

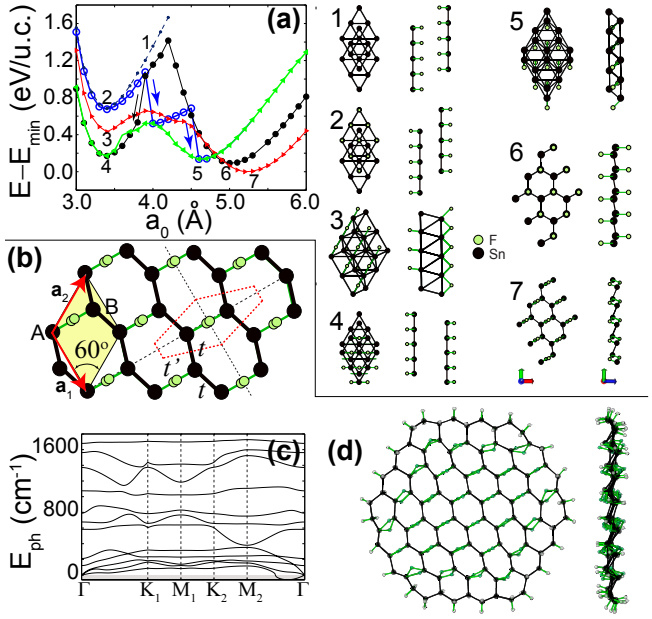

FIG. 4: (Color online.) (a) Phases of 2D fluorinated tin; structures shown to the right. (b) Symmetries of the most stable structure (7), depicting triangular (dashed) and Wigner-Seitz (within dotted perimeter) unit cells, the two symmetry axes, and the two Sn sublattices A and B. Structural stability is demonstrated by (c) phonon dispersion curves and (d) the structural stabilization of a finite-size sample.

TABLE I: Basis vectors for fluorinated stanene ($a_0 = 5.23$ Å).

Sn:	$(0.000, 0.000, 0.000)a_0$,	$(0.583, 0.336, -0.221)a_0$
F:	$(0.216, 0.124, -0.348)a_0$,	$(0.367, 0.212, 0.128)a_0$

$\alpha-$tin– by $E_{LB} - E_{HB} = 0.25$ eV/atom [c.f. Fig. 1(a)].

Fluorinated 2D tin.- The phase space for decorated 2D tin is larger than originally anticipated [Fig. 4(a)]: The graphane-like phase [7, 8] realizes the metastable minima labeled **6** that turns into phase **4** upon in-plane compression. Placement of F atoms directly on top of/under Sn atoms results on two dissociated triangular Sn lattices bonded on opposite sides by F atoms (structures **2**/**1**).

In the optimal structure, **7**, four-fold coordinated Sn atoms form a sequence of parallel zig-zag one-dimensional chains with two fluorine atoms mediating interactions among neighboring Sn chains. The structure is realized on a triangular lattice with $a_0 = 5.230$ Å [Fig. 4(b)]. The Wigner-Seitz unit cell is within the dotted area in Fig. 4(b); the symmetry axes are shown as well. A similar "bridging" fluorine coordination is realized on bulk tin(II) fluoride (e.g., Fig. 2 in Ref. [12]).

Bulk Tin(II) fluoride is highly stable at room temperature and can be found in household products. Structural stability of optimal 2D tin is probed with phonon dispersion calculations [Fig. 4(c)] along the high-symmetry lines shown in Fig. 5(a). The phonon frequency range is comparable with that of graphene, and it is one order-

TABLE II: Eigenvectors of $\tau_z\sigma_x s_x$. $|s_x;\pm\rangle$ are eigenstates of s_x, and $|A\rangle$, $|B\rangle$ are eigenstates of the pseudospin operator.

State	V_1	V_2
$\|\phi_{-\Delta,1}\rangle$:	$\frac{1}{\sqrt{2}}(-\|A\rangle+\|B\rangle)\|s_x;+\rangle$	$\frac{1}{\sqrt{2}}(\|A\rangle-\|B\rangle)\|s_x;-\rangle$
$\|\phi_{-\Delta,2}\rangle$:	$\frac{1}{\sqrt{2}}(\|A\rangle+\|B\rangle)\|s_x;-\rangle$	$-\frac{1}{\sqrt{2}}(\|A\rangle+\|B\rangle)\|s_x;+\rangle$
$\|\phi_{+\Delta,1}\rangle$:	$\frac{1}{\sqrt{2}}(\|A\rangle-\|B\rangle)\|s_x;-\rangle$	$\frac{1}{\sqrt{2}}(-\|A\rangle+\|B\rangle)\|s_x;+\rangle$
$\|\phi_{+\Delta,2}\rangle$:	$\frac{1}{\sqrt{2}}(\|A\rangle+\|B\rangle)\|s_x;+\rangle$	$-\frac{1}{\sqrt{2}}(\|A\rangle+\|B\rangle)\|s_x;-\rangle$

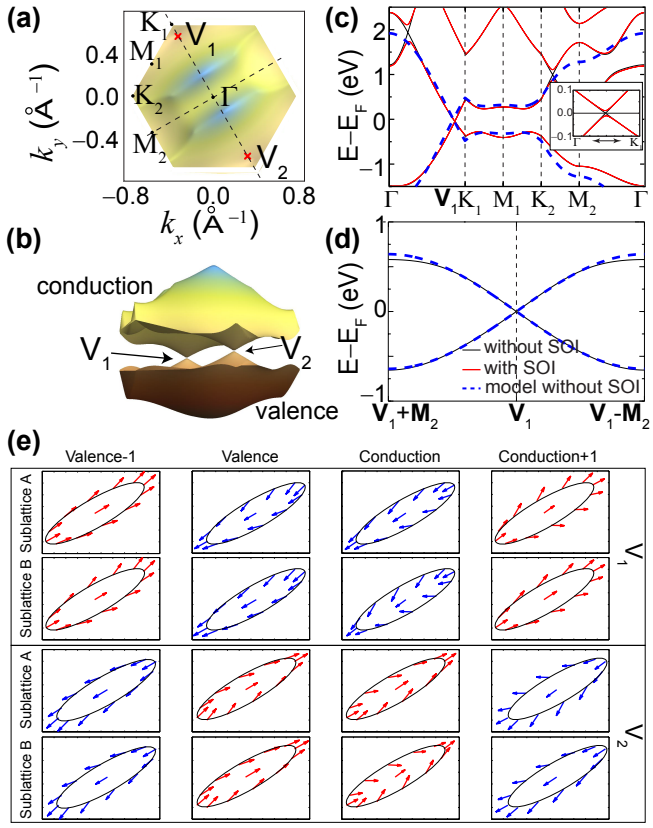

FIG. 5: (Color online.) (a) Conduction band on the first Brillouin zone, highlighting high-symmetry points and locations of valleys $\mathbf{V}_1$ and $\mathbf{V}_2$ away from the K- and K'-points. (b) The two valleys on the Brillouin zone arise from the two-fold symmetry of the atomic structure. (c-d) Band structures along high-symmetry lines, including a two-band tight-binding fit. (e) Spin texture resolved over valley ($\boldsymbol{\tau}$), energy, and sublattice ($\boldsymbol{\sigma}$) degrees of freedom. (The spin projection onto the $z-$axis is of the order of 1% at most.)

of-magnitude larger than those in Fig. 2(a,b). As an additional successful check, small-size flakes were subjected to a successful structural optimization [Fig 4(d)]. The peculiar coupling of quantum degrees of freedom on this system may encourage experimental routes towards the synthesis of 2D fluorinated tin. The stability of its parent 3D compound at room temperature [12, 13] invites experimental investigations of potential viability in 2D.

The first Brillouin zone in Fig. 5(a) shows a top view of the conduction band and the high-symmetry points in momentum space. As seen in Fig. 5(b), the arrangement of parallel 1D Sn wires gives rise to an electronic structure with only two anisotropic Dirac cones on the First Brillouin zone located away from the K-points at positions $\mathbf{V}_1$ and $\mathbf{V}_2 = \pm 0.85\mathbf{K}_1$, respectively. From now on we identify the $x-$axis with the line joining tin atoms across fluorine bridges. The Fermi velocity is close in magnitude to that of graphene and it is anisotropic: $v_{Fy} = 5.4\times10^5$ m/s [Fig. 5(c)], and $v_{Fx} = 2.1\times10^5$ m/s [Fig. 5(d)] and a $2\Delta = 0.02$ eV gap opens due to SOI, five times larger than the intrinsic gap due to SOI in graphene [44]. Phase **6** transitions from a topological insulator to a trivial insulator [8], but the electronic structure of the optimal phase remains robust under larger isotropic strain.

The electronic dispersion in Fig. 5(b-d) can be understood in terms of a 2×2 $\pi-$electron tight-binding Hamiltonian [45] in which an effective coupling t' is set among the tin atoms originally linked by fluorine bridges [thin bonds on Fig. 4(b)], and t is the coupling among actual Sn-Sn atoms [thick bonds on Fig. 4(b)]. Using interatomic distances among Sn atoms from Table I we obtain the blue dashed lines in Fig. 5(c,d) with $t = 0.8$ eV and $t' = \frac{v_{Fx}}{v_{Fy}}t$ which reproduce first-principles results.

To account for SOI, we realize an oblate low-energy Dirac-Hamiltonian at the vicinity of the $\mathbf{V}_{1,2}$ points. The relevant subspace is four-dimensional at any given valley, and the task is to reproduce the spin texture displayed in Fig. 5(e) where spin projects onto the $+x$ or the $-x$ directions while leaving the sublattice (pseudospin) degree of freedom unpolarized. The numerical results on Fig. 5(e) are consistent with a coupling $\tau_z\sigma_x s_x$. Indeed, eigenvectors of $\tau_z\sigma_x s_x$ in Table II project spins onto the $-x$, $+x$, $+x$, $-x$ axis parallel to the Sn-F bonds, inverting signs at each valley and lacking sublattice polarization, consistently with *ab-initio* data [Fig. 5(e)]. Thus, the low-energy dynamics is given by:

$$H = -i\hbar\Psi^\dagger(v_{Fx}\tau_z\sigma_x\partial_x + v_{Fy}\sigma_y\partial_y)\Psi + \Psi^\dagger(\Delta\tau_z\sigma_x s_x)\Psi.$$

An unprecedented specific coupling of momentum – including direction– with spin oriented along $\hat{\mathbf{x}}$ and valley degrees of freedom is thus realized by the second term in previous equation. The valley degree of freedom can be addressed by a bias along the $\mathbf{V}_1-\mathbf{V}_2$ axis that breaks inversion symmetry. Similarly, a magnetic field along the $\hat{\mathbf{x}}$ axis will break time-reversal symmetry, locking the valley and crystal momentum direction at the $\mathbf{V}_1$, $\mathbf{V}_2$ points. The dynamics invites the use of 2D fluorinated tin for valleytronic applications.

We demonstrated the structural stability of HB tin and HB lead and discussed their electronic properties, showed that tin and lead are not viable routes towards topological fullerenes, and discovered the structural, valley, sublattice and spin properties of optimal fluorinated stanene. We are grateful to G. Montambaux, M. Kindermann and L. Bellaiche, and acknowledge the Arkansas Biosciences Institute (P.R. and S.B.L.); the Faculty Development and Research Committee, grant OSPR 140269 and the FCSM Fisher General Endowment at Towson Uni-

versity (J.A.Y.); the Spanish MICINN, grant FIS2012-34858, and European Commission FP7 ITN "MOLESCO," grant number 606728 (V.M.G.S. and J.F.); and a Ramón y Cajal fellowship RYC-2010-06053 (V.M.G.S.). Computations were carried out at Arkansas and TACC (XSEDE TG-PHY090002).

[1] M. Katsnelson, *Graphene: Carbon in Two Dimensions* (Cambridge U. Press, 2012), 1st ed.
[2] A. H. Castro Neto, F. Guinea, N. M. R. Peres, K. S. Novoselov, and A. K. Geim, Rev. Mod. Phys. **81**, 109 (2009).
[3] S. Cahangirov, M. Topsakal, E. Aktürk, H. Sahin, and S. Ciraci, Phys. Rev. Lett. **102**, 236804 (2009).
[4] H. Zhuang, A. Singh, and R. Hennig, Phys. Rev. B **87**, 165415 (2013).
[5] Z. Zhu and D. Tománek, Phys. Rev. Lett. **112**, 176802 (2014).
[6] J. C. Garcia, D. B. de Lima, L. V. C. Assali, and J. F. Justo, J. Phys. Chem. C **115**, 13242 (2011).
[7] Y. Ma, Y. Dai, M. Guo, C. Niu, and B. Huang, J. Phys. Chem. C **116**, 12977 (2012).
[8] Y. Xu, B. Yan, H.-J. Zhang, J. Wang, G. Xu, P. Tang, W. Duan, and S.-C. Zhang, Phys. Rev. Lett. **111**, 136804 (2013).
[9] N. Roome and J. Carey, ACS Appl. Mater. Interfaces **6**, 7743 (2014).
[10] B. van den Broek, M. Houssa, E. Scalise, G. Pourtois, V. V. Afanas'ev, and A. Stesmans, 2D Materials **1**, 021004 (2014).
[11] J. Sofo, A. Chaudhari, and G. Barber, Phys. Rev. B **75**, 153401 (2007).
[12] R. C. McDonald, H. H.-K. Hau, and K. Eriks, Inorg. Chem. **15**, 762 (1976).
[13] G. Denes, J. Pannetier, J. Lucas, and J. Y. Le Marouille, J. Solid State Chem. **30**, 335 (1979).
[14] C. Kane and E. Mele, Phys. Rev. Lett. **95**, 226801 (2005).
[15] A. Rycerz, J. Tworzydlo, and C. W. J. Beenakker, Nat. Phys. **3**, 172 (2007).
[16] D. Xiao, W. Yao, and Q. Niu, Phys. Rev. Lett. **99**, 236809 (2007).
[17] J. Jung, F. Zhang, Z. Quiao, and A. H. McDonald, Phys. Rev. B **84**, 075418 (2011).
[18] Y. Jiang, T. Low, K. Chang, M. I. Katsnelson, and F. Guinea, Phys. Rev. Lett. **110**, 046601 (2013).
[19] X. Xu, W. Yao, D. Xiao, and T. Heinz, Nat. Phys. **10**, 343 (2014).
[20] J. Perdew, K. Burke, and M. Ernzerhof, Phys. Rev. Lett. **77**, 3865 (1996).
[21] J. Soler, E. Artacho, J. Gale, A. García, J. Junquera, P. Ordejón, and D. Sánchez-Portal, J. Phys.: Condens. Matter **14**, 2745 (2002).
[22] E. Artacho, E. Anglada, O. Dieguez, J. Gale, A. García, J. Junquera, R. Martin, P. Ordejón, J. Pruneda, D. Sánchez-Portal, et al., J. Phys.: Condens. Matter **20**, 064208 (2008).
[23] L. Fernandez-Seivane, M. A. Oliveira, S. Sanvito, and J. Ferrer, J. Phys.: Condens. Matter **18**, 7999 (2006).
[24] P. Rivero, V. García-Suárez, Y. Yang, L. Bellaiche, K. Park, J. Ferrer, and S. Barraza-Lopez, Submitted (2014).
[25] G. Kresse and J. Hafner, Phys. Rev. B **47**, 558 (1993).
[26] G. Kresse and J. Hafner, Phys. Rev. B **49**, 14251 (1994).
[27] M. Marder, *Condensed Matter Physics* (Wiley-Interscience, 2000), 1st ed.
[28] C. Sabater, D. Gosálbez-Martínez, J. Fernández-Rossier, J. Rodrigo, C. Untiedt, and J. Palacios, Phys. Rev. Lett. **110**, 176802 (2013).
[29] L. Miao, Z. Wang, M.-Y. Yao, F. Zhu, J. Dil, C. Gao, C. Liu, F. Liu, D. Quian, and J. Jia, Phys. Rev. B **89**, 155116 (2014).
[30] Phonon dispersion calculations were performed with the Vibra tool. The atomic displacements used in computing force constants were as small as 0.01 Å, we set the electronic tolerance smaller than 10^{-5} eV, and the mesh cutoff for the real-space grid was larger than 800 Ry. Large supercells were needed in order to eliminate spurious negative frequencies, and a $11\times11\times1$ ($13\times13\times1$) supercell containing 242 (338) atoms for the calculations of high-buckled tin (lead). Due to a heavier computational cost, the calculations that included SOI were carried out on $9\times9\times1$ supercells, containing 162 atoms. A $k-$point sampling of at least $6\times6\times1$ in all phonon calculations ensures a properly converged electronic density.
[31] Phonon dispersion calculations with the Quantum Espresso package [32] confirm these results.
[32] P. Giannozzi, S. Baroni, N. Bonini, M. Calandra, R. Car, C. Cavazzoni, D. Ceresoli, G. L. Chiarotti, M. Cococcioni, I. Dabo, et al., J. Phys.: Condens. Matter **21**, 395502 (2009).
[33] A. Rüegg, S. Coh, and J. Moore, Phys. Rev. B **88**, 155127 (2013).
[34] T. Ando, J. Phys. Soc. Jpn. **69**, 1757 (2000).
[35] D. Huertas-Hernando, F. Guinea, and A. Brataas, Phys. Rev. B **74**, 155426 (2006).
[36] C.-C. Liu, W. Feng, and Y. Yao, Phys. Rev. Lett. **107**, 076802 (2011).
[37] C.-C. Liu, H. Jiang, and Y. Yao, Phys. Rev. B **84**, 195430 (2011).
[38] A. Barfuss, L. Dudy, M. Scholz, H. Roth, P. Höpfner, C. Blumenstein, G. Landolt, J. Dil, N. Plumb, M. Radovic, et al., Phys. Rev. Lett. **111**, 157205 (2013).
[39] Y. Ohtsubo, P. Le Fébre, F. Bertran, and A. Taleb-Ibrahimi, Phys. Rev. Lett. **111**, 216401 (2013).
[40] T. Miller, M. Y. Chou, and T.-C. Chiang, Phys. Rev. Lett. **102**, 236803 (2009).
[41] P. Bridman, Proc. Am. Acad. Arts Sci. **60**, 305 (1925).
[42] P. Pavone, S. Baroni, and S. de Gironcoli, Phys. Rev. B **57**, 10421 (1998).
[43] J. Chelikowsky and M. Cohen, Phys. Rev. B **14**, 556 (1976).
[44] D. Huertas-Hernando, F. Guinea, and A. Brataas, Phys. Rev. B **74**, 155426 (2006).
[45] G. Montambaux, F. Piéchon, J. Fuchs, and M. Goerbig, Phys. Rev. B **80**, 153412 (2009).